(Invited) Multi-Channel AlGaN/GaN Power Rectifiers: Breakthrough Performance up to 10 kV

Y. Zhang^{a*}, M. Xiao^a, Y. Ma^a, Z. Du^b, H. Wang^b, A. Xie^c, E. Beam^c, Y. Cao^c, and K. Cheng^d

^a Center for Power Electronics Systems, Virginia Polytechnic Institute and State University, Virginia 24060, USA

^b Ming Hsieh Department of Electrical and Computer Engineering, University of Southern California, California 90089, USA

^c Qorvo Inc., Texas 75081, USA ^d Enkris Semiconductor Inc., Jiangsu 215123, China *E-mail: yhzhang@vt.edu

High-voltage power rectifiers are widely used in renewable energy processing, electric grids, industrial motor drives, pulse power systems, among other applications. Today's high-voltage rectifier market is dominated by bipolar Si diodes up to 6.5 kV, which suffer from slow reverse recovery. Wide-bandgap SiC unipolar diodes have been pre-commercialized up to 10 kV, which allows for a much higher switching speed. Recently, we have developed a new generation of high-voltage rectifiers based on the multichannel AlGaN/GaN platform, which highlight a series of novel device designs incorporating the stacked two-dimensional electron gas (2DEG) channels, p-n junctions, and 3-D fin structures. With these innovations, the performances of our unipolar 1.2-10 kV multi-channel AlGaN/GaN Schottky rectifiers well exceed the Si and SiC 1-D limit, at the same time possessing a lower cost as compared to SiC counterparts. This paper reviews our efforts in the design, fabrication and characterization of these GaN devices. Our results show the tremendous promise of GaN for medium-voltage and high-voltage power electronics applications.

Introduction

Power semiconductor devices providing low on-resistance, high switching speed, and high blocking voltage are central to improving the efficiency of electrical energy processing in electric vehicles, data centers, electric grids, among other applications. High-voltage (HV, 1.7 kV – 10 kV) power rectifiers are ubiquitously used in electricity grid, renewable energy processing, industrial motors, and electrified transportation (Fig. 1). Today's HV rectifier market is dominated by bipolar Si p-n junction diodes up to 6.5 kV. However, they have a very slow switching speed due to poor reverse recovery. A superior alternative that allows fast switching is the SiC Schottky barrier diode (SBD) or junction Schottky barrier (JBS) diode. SiC JBS diodes up to 10 kV have been precommercialized by Cree/Wolfspeed (1) and used in R&D power electronics applications (2-4). However, the epitaxial and fabrication costs of HV SiC rectifiers are much higher than Si counterparts, which hinder their wide adoption and commercialization.

Another material that offers superior physical properties for power devices is GaN. Compared to Si and SiC, GaN has a higher critical electric field (E-field) and a unique high-mobility channel, the two-dimensional electron gas (2DEG). After two decades of development, lateral GaN power devices have been commercialized up to 650 V as a superior replacement of the similarly-rated Si devices (5,6). However, the continued voltage and power upscaling of lateral GaN devices have encountered great challenges, many of which stem from the limited current capability of the thin 2DEG channel, crowded E-field near the device surface, and the resulted difficulties in thermal management (7,8). Despite the reports of high-voltage lateral GaN SBDs up to 9 kV (9,10), their differential on-resistance is significantly larger than that of SiC SBDs. This situation leads to a common belief that the vertical GaN structure is more favorable for HV power devices. However, despite many high-performance vertical GaN devices at 1.2-2 kV classes (11-13), the highest breakdown voltage (*BV*) reported in vertical GaN devices is only 5 kV (14).

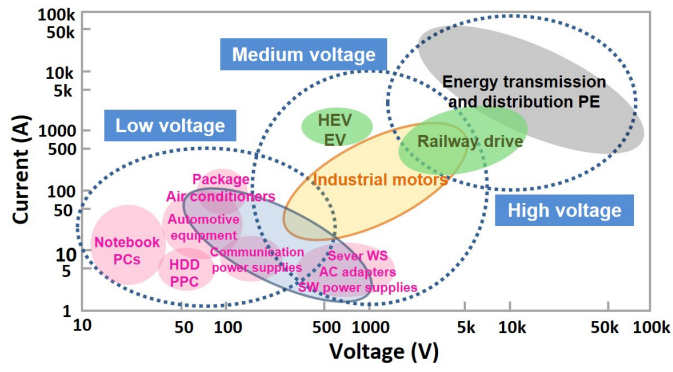


Figure 1. Representative applications of low-, medium- and high-voltage power rectifiers.

Recently, our team has proposed the multi-channel lateral AlGaN/GaN platform for HV power devices and demonstrated a series of novel lateral GaN rectifiers that feature stacked 2DEG channels and innovative device designs. The fundamental rational to pursue multi-channel AlGa/GaN devices is that they retain a high 2DEG mobility while concurrently leveraging the benefits of vertical devices, e.g., spatially-distributed electron current and E-field, to maximize the power density. Our devices are fabricated on 4-inch AlGaN/GaN-on-sapphire wafers that host five stacked 2DEG channels and have a sheet resistance ($R_{\rm SH}$) below 120 Ω /sq, which is at least 4~5-fold lower than that in commercial lateral GaN devices. The cost of this GaN-on-sapphire wafer is estimated to be 2~3-fold lower than a SiC wafer (6). However, voltage upscaling in multi-channel devices is more challenging than that in the single-channel counterpart, due to the excess charges and the resulted leakage current and E-field crowding. To overcome these challenges, we have demonstrated various device innovations, including the p-GaN edge termination (15), 3-D junction-fin anode (16), and p-GaN reduced surface field (RESURF) structure (17). With these innovations, the performance of our multi-channel AlGaN/GaN rectifiers up to 10 kV has well exhibited the unipolar 1-D limit of SiC devices.

Large-Diameter Multi-Channel Wafer

Power device design aims at concurrent realization of lower on-resistance ($R_{\rm ON}$) and high BV. By stacking multiple 2DEG channels, the 2DEG density can be increased proportionally, therefore reducing the wafer $R_{\rm SH}$ and device $R_{\rm ON}$. AlGaN/GaN multi-

channel epitaxy has been initially demonstrated around the 2010s by Molecular Beam Epitaxy (MBE) (18). However, MBE is usually not suitable for large-diameter, high-volume wafer production. Recently, 4-inch multi-channel wafers have become available by Metal-Organic Vapour-Phase Epitaxy (MOCVD) on various substrates including Si, SiC, sapphire and GaN. The 4-inch, 5-channel, GaN-on-sapphire wafer produced by Enkris Semiconductor Inc. (Fig. 2) possesses a 2DEG density of 3.7×10^{13} cm⁻², a 2DEG mobility of 1475 cm²/V·s, and an R_{SH} of 110 Ω /sq, with the R_{SH} being over 3-fold lower than the usual value of a single-channel wafer. A p-GaN cap layer can be continuously grown on the multi-channel AlGaN/GaN structure (17). Even with the p-GaN depletion, the multi-channel wafer retains a 2DEG density of 1.75×10^{13} cm⁻², a 2DEG mobility of 2010 cm²/V·s, and an R_{SH} of 178 Ω /sq. This low R_{SH} is key to enabling a device R_{ON} much lower than that of similarly-rated SiC and Si rectifiers.

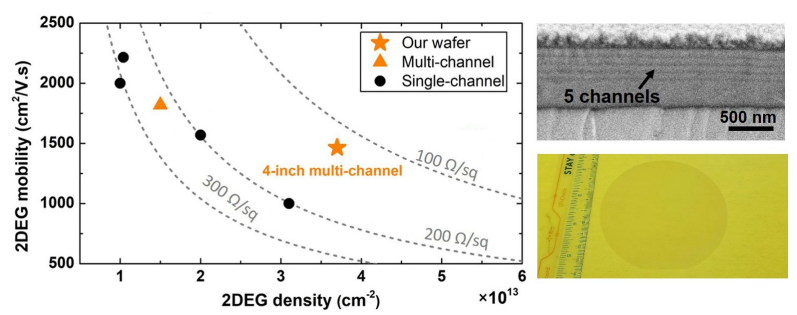


Figure 2. Comparison the 2DEG properties of our wafer with other reports. Scanning electron microscopy image showing 5 channels, and a photo of the large-diameter wafer.

P-GaN Termination: E-field Management

The excess charges from multiple 2DEG channels often induce E-field crowding, and this issue is particularly crucial for Schottky rectifiers, as their BV is typically limited by the peak E-field at the Schottky contact region. Proper edge termination is thus essential to alleviate the E-field crowding or potentially move the peak E-field away from the Schottky contact, just like the basic principle of the JBS design (19,20). For lateral AlGaN/GaN SBDs, field plate is a widely-used edge termination structure (Fig. 3(a)). However, its effectiveness requires precise control over the field plate geometry, such as dielectric thickness and field plate length. Additionally, the complex interfaces between dielectrics and semiconductors often result in device instability under high E-field, leading to preliminary breakdown.

To address the above challenges, we developed a new termination structure using a p-GaN layer epitaxially grown on AlGaN/GaN (Fig. 3(b)) (15). Owing to the vertical depletion enabled by the p-n junction, the E-field lines spreads out, and their distribution becomes more uniform. The peak electric field is also moved from the Schottky contact to the edge of p-GaN, thereby shielding the Schottky contact from high E-field. Compared to the field plate, this p-GaN termination possesses a wide design window in terms of doping concentration and thickness and comprises few dielectric interfaces. Its fabrication is fully compatible with today's foundry process for manufacturing the p-gate normally-off high-electron-mobility transistors (HEMTs), thereby opening the possibilities for integrating high-voltage rectifiers with GaN power ICs. This p-GaN termination structure enables the demonstration of the first 3.3-kV AlGaN/GaN multichannel SBDs exceeding the SiC unipolar limit (15).

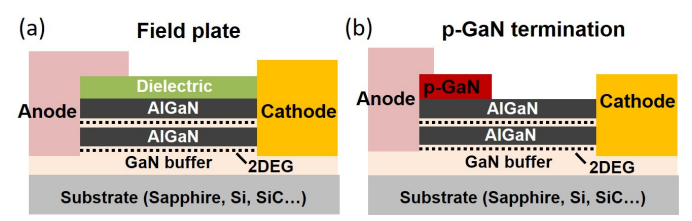


Figure 3. Schematic of (a) field plate and (b) p-GaN termination for multi-channel AlGaN/GaN SBDs.

P-GaN RESURF: Towards the Multi-Channel Super-Junction

Superjunction is one of the most successful concepts in the history of power device development, which relies on alternative n- and p-doped pillars and can break the theoretical trade-off between $R_{\rm ON}$ and BV of 1-D drift regions (21). In GaN, the vertical superjunction like that in Si and SiC has not been experimentally demonstrated (22,23). An alternative superjunction in lateral GaN relying on the natural balance in polarization charges, which is referred to as "polarization superjunction" or "natural superjunction", has been experimentally demonstrated on single- or double-channels (10,24). However, the reported performance of GaN polarization superjunction devices is not significantly better than the 1-D counterparts, and the $R_{\rm ON}$ vs. BV trade-off is inferior to SiC devices.

In an undoped multi-channel structure, according to the ideal band theories, a balance in polarization charges is expected to be naturally established in each channel, thereby forming a multi-channel polarization superjunction. If this is true, a p-GaN termination would be sufficient for E-field management, and the E-field distribution in the access region should be quite uniform benefited from the superjunction properties. However, the net charge in our experimental multi-channel devices was found to be non-zero, and the additional donors are present. To reach the overall charge balance in this "unbalanced superjunction", we proposed a novel design for multi-channel devices, the p-GaN RESURF structure (Fig. 4(a)). Compared to the p-GaN termination, the p-GaN RESURF layer extends to the region nearing the cathode, and its total acceptor charges balance the net donor charges in the multi-channel structure when the device is blocking voltage (Fig. 4(b)) (17). In the fabrication, C-V measurements on a test structure along with the p-GaN etch can identify the critical p-GaN thickness to reach the overall charge balance (17).

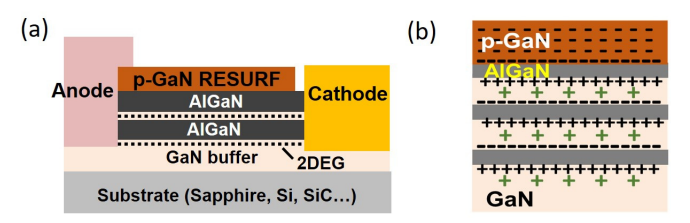


Figure 4. Schematic of the (a) RESURF multi-channel AlGaN/GaN SBD and (b) charge balance in this RESURF multi-channel structure.¹⁷

Fig. 5(a) and (b) show the forward characteristics of the p-GaN-terminated SBDs with an anode-to-cathode distance ($L_{\rm AC}$) of 98-148 µm and the p-GaN RESURF SBDs with $L_{\rm AC}$ of 48-123 µm. A same turn-on voltage ($V_{\rm on}$) was extracted to be 0.6 V for all SBDs A low on-resistance ($R_{\rm on}$) of 28.7 and 31 Ω ·mm was extracted in the p-GaN

RESURF SBDs with 98 and 123 μ m L_{AC} , respectively. Fig. 5(c) shows reverse I-V characteristics of the three types of SBDs with increased L_{AC} . With an identical L_{AC} (e.g., 98 μ m), the p-GaN RESURF SBD shows a BV about 2-fold higher than that of the SBD without edge termination and about 1.5-fold higher than that of the SBD with p-GaN termination. Despite the non-uniform E-field, an average lateral E-field ($E_{AVE} = BV/L_{AC}$) can be calculated, which is useful for the lateral device design. At a BV of \sim 5 kV and above, the E_{AVE} of non-terminated SBDs, p-GaN-terminated SBDs, and p-GaN RESURF SBDs are 0.42-0.47 MV/cm, 0.59-0.64 MV/cm, 0.94-1 MV/cm, respectively. The p-GaN RESURF SBD with 98 μ m L_{AC} shows a BV of 9.15 kV; the device with 123 μ m L_{AC} was measured to 10 kV (our measurement limit) repeatedly without showing any degradation.

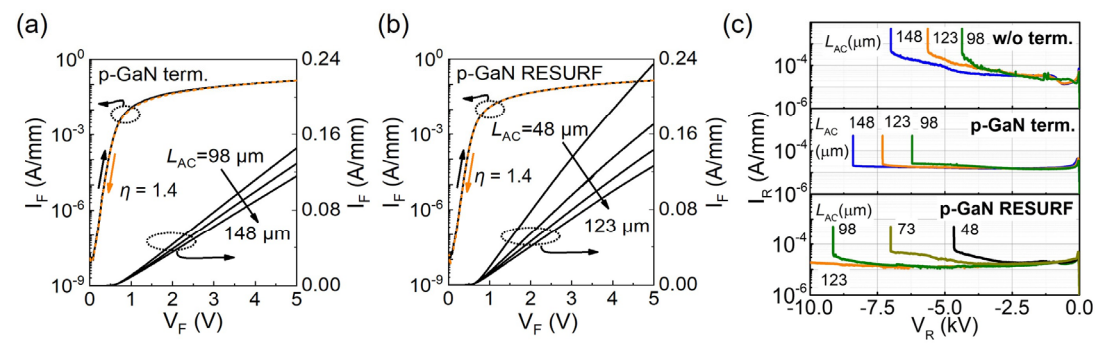


Figure 5. Forward I-V characteristics of multi-channel AlGaN/GaN SBDs with various L_{AC}, one with (a) p-GaN termination and (b) the other with p-GaN RESURF structures.
(c) Reverse I-V characteristics at various L_{AC} for multi-channel SBDs with and without terminations as well as with the ones with p-GaN termination or p-GaN RESURF.

The SBD with a 98- μ m L_{AC} shows a BV of 9.15 kV and a specific R_{ON} of 29.5 m $\Omega \cdot \text{cm}^2$, rendering a Baliga's figure of merit (FOM= BV^2/R_{ON}) of 2.84 GW/cm². The SBD with a 123- μ m L_{AC} shows a BV over 10 kV and a R_{ON} of 39 m $\Omega \cdot \text{cm}^2$, which is 2.5-fold lower than the R_{ON} of the state-of-the-art 10-kV SiC JBS diodes. The Baliga's FOMs of our 4.6-10 kV GaN SBDs well exceed the SiC unipolar limit.

Junction-Fin Anode: Minimizing the Leakage Current

The leakage current reduction is another challenge facing high-voltage multi-channel devices, as the Schottky contact to each AlGaN/GaN channel may suffer from barrier lowering effect subject to high bias. Addressing this challenge is our junction-fin-anode, a three-dimensional anode structure that comprises p-n junctions wrapping around the multi-2DEG-fins (Fig. 6(a)) (16). Compared to the planar p-GaN termination or RESURF structure, the 3-D wrapped p-n junctions can provide a stronger depletion of the 2DEG channel. When the device is reverse biased, the junction-fin assists the Schottky contact for charge depletion and shields the Schottky contact from seeing high biases.

Our design can be illustrated by the equivalent circuit model of the entire rectifier (Fig. 6(b)) This model includes an equivalent series connection for a sidewall SBD, a junction-fin-gated HEMT, and a p-gate HEMT. As the reverse bias increases, the sidewall SBD is pinched off, and then the two HEMTs. The voltage drop on the sidewall SBD is clamped at the threshold voltage of the junction-fin-gated HEMT, which is merely a few volts. This clamping occurs regardless of the reverse bias at the cathode,

which can reach thousands of volts. Operating in this manner, the leakage current of the entire rectifier is equal to that of one of the sidewall SBDs biased at a few volts.

In our prototyped 5-kV device, we realized the junction-fin structure by regrowth of p-GaN on top of the fin, and the addition of a p-type nickel oxide at the fin sidewalls (16). The resulting rectifier delivers a BV up to 5.2 kV, and when operating at 90% of this BV, the leakage current is just 1.4 μ A/mm. The specific $R_{\rm ON}$ is 13.5 m Ω ·cm², rendering a power figure-of-merit (FOM) exceeding the SiC unipolar limit. Subsequently, large-area multi-channel AlGaN/GaN SBDs with junction-fin anodes have been fabricated. They are capable of handling a 1.5 A current, have a leakage current measured in microamps, and a total charge of 13 nC (Fig. 6(c)-(d)). As compared with commercial and R&D SiC SBDs with similar voltage and current ratings, our multi-channel GaN SBDs exhibit a significantly lower forward voltage and charges.

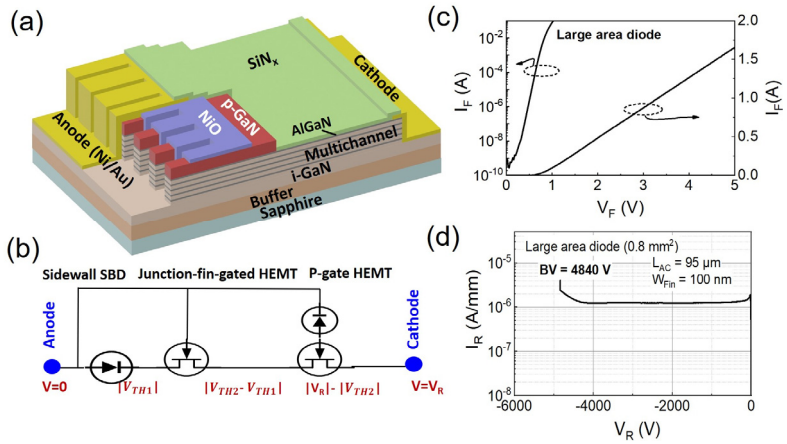


Figure 6. (a) 3-D schematic and (b) equivalent circuit model of the multi-channel AlGaN/GaN SBDs with the junction-fin anode. (c) Forward and (d) reverse I-V characteristics of the fabricated large-area devices.

We note that the junction-fin anode structure can be not only compatible to the p-GaN termination structure as we demonstrated in (16) but also the RESURF structure. To showcase this viability, we scrutinized the functions of the p-GaN termination and junction-fin anode. As shown in Fig. 7, the p-GaN termination determines the device BV, while the junction-fin-anode reduces the leakage current. This suggests, by combining the p-GaN RESURF and junction-fin anode in multi-channel devices, a further reduction of leakage current can be readily envisioned in 10-kV+ multi-channel AlGaN/GaN SBDs.

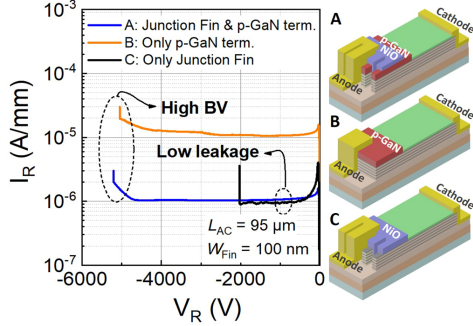


Figure 7. Reverse I-V characteristics of devices with only p-GaN termination, only junction-fin, and both structures.

Benchmark and Summary

Fig. 8 benchmarks the specific $R_{\rm ON}$ vs. BV of our multi-channel AlGaN/GaN SBDs with the state-of-the-art GaN SBDs, SiC JBS/SBDs, and Ga₂O₃ SBDs with a BV over 2 kV. A contact finger length of 3 μ m (25) was added to $L_{\rm AC}+L_{\rm A}$ in $R_{\rm ON,SP}$ calculation. Our 1.2-10 kV multi-channel SBDs show a Baliga's FOM ($BV^2/R_{\rm ON}$) of over 2.8 GW/cm², which is the highest among all reported multi-kilovolts SBDs and well exceeds the 1-D SiC unipolar limit. The practical performance limit of AlGaN/GaN multi-channel devices $[R_{on,sp} = BV^2/(q\mu_{2DEG}n_{2DEG}E_{AVE}^2)]$ was found to reach the vertical GaN limit using $E_{\rm AVE} = 1$ MV/cm and $R_{\rm SH} = 150$ Ω /sq.

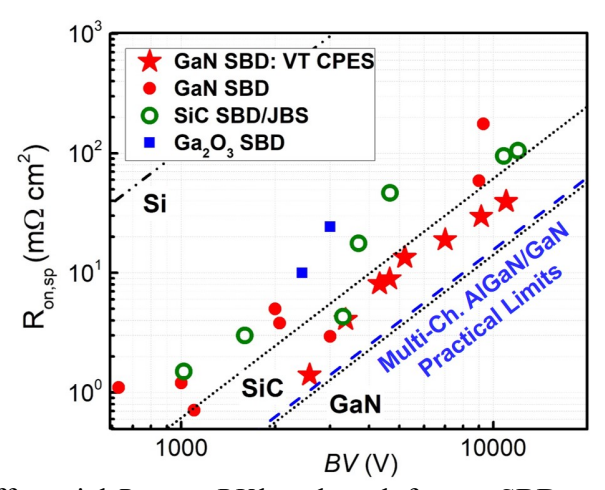


Figure 8. The differential *R*_{ON} *vs. BV* benchmark for our SBDs and the state-of-theart GaN, SiC, and Ga₂O₃ HV SBDs. The Si, SiC, GaN bulk limits and the multi-channel lateral AlGaN/GaN practical limit are also plotted.

In particular, our multi-channel RESURF SBD with a 123- μ m L_{AC} shows a BV over 10 kV and a R_{ON} of 39 m Ω ·cm², which is 2.5-fold lower than the R_{ON} of the state-of-the-art 10-kV SiC JBS diodes. In addition, our 10-kV GaN SBD has a V_{ON} (0.6 V) lower than that of 10-kV SiC JBS diode (>1 V (26)), suggesting a lower forward voltage (V_F). Assuming an 80 mA/mm forward current, the switching FOM (V_F · Q_C) of a 10-kV, 0.3-A GaN multi-channel RESURF SBD is projected to be 15.7 nC·V, which is even lower than that of a commercial 3.3-kV, 0.3-A SiC SBD (30.8 nC·V, GAP3SLT33-214 GeneSiC Semiconductor) (no Q_C data available for higher-voltage SiC SBDs).

These superior device performances, in addition to the lower wafer and fabrication cost of lateral GaN devices, all show the great potential of pushing GaN power devices into the HV realm and the good promise of the multi-channel AlGaN/GaN devices as the platform technology for HV GaN devices.

Acknowledgments

The Virginia Tech authors acknowledge the partial support by the National Science Foundation under Grant ECCS-2036740 and the Power Management Industry Consortium of the Center for Power Electronics Systems, Virginia Tech.

References

- 1. J. B. Casady, V. Pala, D.J. Lichtenwalner, E.V. Brunt, B. Hull, G. Wang, J. Richmond, S.T. Allen, D. Grider, and J.W. Palmour, in *Proc. PCIM Eur. 2015 Int. Exhib. Conf. Power Electron. Intell. Motion Renew. Energy Energy Manag.* (2015), pp. 1–8.
- 2. J. Wang, T. Zhao, J. Li, A.Q. Huang, R. Callanan, F. Husna, and A. Agarwal, *IEEE Trans. Electron Devices* **55**, 1798 (2008).
- 3. R. Zhang, X. Lin, J. Liu, S. Mocevic, D. Dong, and Y. Zhang, *IEEE Trans. Power Electron.* **36**, 2033 (2021).
- 4. R. Zhang, X. Lin, J. Liu, S. Mocevic, D. Dong, and Y. Zhang, in 2020 32nd Int. Symp. Power Semicond. Devices ICs ISPSD (2020), pp. 246–249.
- 5. Y. Zhang, A. Zubair, Z. Liu, M. Xiao, J.A. Perozek, Y. Ma, and T. Palacios, *Semicond. Sci. Technol.* **36**, 054001 (2021).
- 6. Y. Zhang, A. Dadgar, and T. Palacios, J. Phys. Appl. Phys. 51, 273001 (2018).
- 7. Y. Zhang, M. Sun, Z. Liu, D. Piedra, H.S. Lee, F. Gao, T. Fujishima, and T. Palacios, *IEEE Trans. Electron Devices* **60**, 2224 (2013).
- 8. Y. Zhang and T. Palacios, IEEE Trans. Electron Devices 67, 3960 (2020).
- 9. A. Colón, E.A. Douglas, A.J. Pope, B.A. Klein, C.A. Stephenson, M.S. Van Heukelom, A. Tauke-Pedretti, and A.G. Baca, *Solid-State Electron*. **151**, 47 (2019).
- 10. H. Ishida, D. Shibata, H. Matsuo, M. Yanagihara, Y. Uemoto, T. Ueda, T. Tanaka, and D. Ueda, in *2008 IEEE Int. Electron Devices Meet. IEDM* (2008), pp. 1–4.
- 11. Y. Zhang, M. Sun, J. Perozek, Z. Liu, A. Zubair, D. Piedra, N. Chowdhury, X. Gao, K. Shepard, and T. Palacios, *IEEE Electron Device Lett.* **40**, 75 (2019).
- 12. J. Liu, M. Xiao, Y. Zhang, S. Pidaparthi, H. Cui, A. Edwards, L. Baubutr, W. Meier, C. Coles, and C. Drowley, in 2020 IEEE Int. Electron Devices Meet. IEDM (2020), p. 23.2.1-23.2.4.
- 13. J. Liu, M. Xiao, R. Zhang, S. Pidaparthi, H. Cui, A. Edwards, M. Craven, L. Baubutr, C. Drowley, and Y. Zhang, *IEEE Trans. Electron Devices* **68**, 2025 (2021).
- 14. H. Ohta, K. Hayashi, F. Horikiri, M. Yoshino, T. Nakamura, and T. Mishima, *Jpn. J. Appl. Phys.* **57**, 04FG09 (2018).
- 15. M. Xiao, Y. Ma, K. Cheng, K. Liu, A. Xie, E. Beam, Y. Cao, and Y. Zhang, *IEEE Electron Device Lett.* 41, 1177 (2020).
- 16. M. Xiao, Y. Ma, Z. Du, X. Yan, R. Zhang, K. Cheng, K. Liu, A. Xie, E. Beam, Y. Cao, H. Wang, and Y. Zhang, in 2020 IEEE Int. Electron Devices Meet. IEDM (2020), p. 5.4.1-5.4.4.
- 17. M. Xiao, Y. Ma, K. Liu, K. Cheng, and Y. Zhang, *IEEE Electron Device Lett.* **42**, 808 (2021).
- 18. Y. Cao, K. Wang, G. Li, T. Kosel, H. Xing, and D. Jena, *J. Cryst. Growth* **323**, 529 (2011).
- 19. Y. Zhang, Z. Liu, M.J. Tadjer, M. Sun, D. Piedra, C. Hatem, T.J. Anderson, L.E. Luna, A. Nath, A.D. Koehler, H. Okumura, J. Hu, X. Zhang, X. Gao, B.N. Feigelson, K.D. Hobart, and T. Palacios, *IEEE Electron Device Lett.* **38**, 1097 (2017).

- 20. Y. Zhang, M. Sun, Z. Liu, D. Piedra, M. Pan, X. Gao, Y. Lin, A. Zubair, L. Yu, and T. Palacios, in 2016 IEEE Int. Electron Devices Meet. IEDM (2016), p. 10.2.1-10.2.4.
- 21. F. Udrea, G. Deboy, and T. Fujihira, *IEEE Trans. Electron Devices* **64**, 720 (2017).
- 22. M. Xiao, R. Zhang, D. Dong, H. Wang, and Y. Zhang, *IEEE J. Emerg. Sel. Top. Power Electron.* 7, 1475 (2019).
- 23. Y. Ma, M. Xiao, R. Zhang, H. Wang, and Y. Zhang, *IEEE J. Electron Devices Soc.* 8, 42 (2020).
- 24. H. Ishida, D. Shibata, M. Yanagihara, Y. Uemoto, H. Matsuo, T. Ueda, T. Tanaka, and D. Ueda, *IEEE Electron Device Lett.* **29**, 1087 (2008).
- 25. R. Zhang, J.P. Kozak, M. Xiao, J. Liu, and Y. Zhang, *IEEE Trans. Power Electron.* **35**, 13409 (2020).
- 26. J. Lynch, N. Yun, and W. Sung, in 2019 31st Int. Symp. Power Semicond. Devices ICs ISPSD (2019), pp. 223–226.